Neutron Powder Diffraction and Molecular Simulation Study of the Structural Evolution of Ammonia Borane from 15 to 340 K

Nancy J. Hess,*,† Gregory K. Schenter,† Michael R. Hartman,‡ Luc L. Daemen,§ Thomas Proffen,§ Shawn M. Kathmann,† Christopher J. Mundy,† Monika Hartl,§ David J. Heldebrant,† Ashley C. Stowe,† and Tom Autrey†

Pacific Northwest National Laboratory, Richland, Washington 99352, University of Michigan, Ann Arbor, Michigan 48109, and Los Alamos National Laboratory, Los Alamos, New Mexico 87545

Received: January 28, 2009; Revised Manuscript Received: March 20, 2009

The structural behavior of ^{11}B-, ^{2}H-enriched ammonia borane, $ND_3{}^{11}BD_3$, over the temperature range from 15 to 340 K was investigated using a combination of neutron powder diffraction and ab initio molecular dynamics simulations. In the low temperature orthorhombic phase, the progressive displacement of the borane group under the amine group was observed leading to the alignment of the B−N bond near parallel to the *c*-axis. The orthorhombic to tetragonal structural phase transition at 225 K is marked by dramatic change in the dynamics of both the amine and borane group. The resulting hydrogen disorder is problematic to extract from the metrics provided by Rietveld refinement but is readily apparent in molecular dynamics simulation and in difference Fourier transform maps. At the phase transition, Rietveld refinement does indicate a disruption of one of two dihydrogen bonds that link adjacent ammonia borane molecules. Metrics determined by Rietveld refinement are in excellent agreement with those determined from molecular simulation. This study highlights the valuable insights added by coupled experimental and computational studies.

Introduction

Ammonia borane, NH_3BH_3, is a unique molecular complex that is formed in the reaction between ammonia and a borane solvent complex.[1] Bond formation between the electron-rich NH_3 and electron-deficient BH_3 results in a dative bond complex ($H_3N{\rightarrow}BH_3$) with a dipole moment of 5.1 D. The polar NH_3BH_3 molecule is isoelectronic with ethane. However, unlike ethane, ammonia borane is a solid at standard conditions due in part to dipole−dipole interactions and to a network of "dihydrogen bonds" where the hydridic hydrogen attached to the boron acts as a hydrogen acceptor for the protonic hydrogen attached to nitrogen.[2] The molecular crystalline solid undergoes an orthorhombic to tetragonal phase transition at 225 K.[3] Above 340 K, there is an additional phase transformation from the crystalline tetragonal solid to the polymer $(BH_2NH_2)_n$ and H_2 is rapidly released.[4−6] Due to its high hydrogen content, >19 wt % hydrogen, and the relatively low temperature at which H_2 is released, <350 K, ammonia borane is being given serious consideration as a solid state hydrogen storage material.[7] This study follows the structural changes in ammonia borane across the 225 K phase transition using coupled analysis of the neutron powder diffraction data and ab initio molecular dynamics simulations to characterize the internal molecular geometry and hydrogen disorder and its impact on the dihydrogen bonding network as a function of temperature.

The nature of the order−disorder transition in ammonia borane was first described, and the atomic positions of the boron and nitrogen atoms were determined using X-ray diffraction in the low temperature, orthorhombic phase by Hoon and Reynhard.[3] Later, a neutron diffraction study using a single crystal of NH_3BH_3 reversed the boron and nitrogen atomic positions and located the hydrogen atoms in the orthorhombic unit cell.[2] The revised boron and nitrogen positions resulted in intermolecular BH···H and NH···H bond angles that were consistent with other compounds with dihydrogen bonds.[2] Recently, two characterizations of the room temperature, tetragonal phase of ammonia borane using neutron powder[8] and X-ray single crystal[9] have been conducted. Both studies use an 8-site model to describe the hydrogen atom disorder in the amine and borane groups, which provides a mathematical description of the diffraction data but does not preserve the molecular symmetry of ammonia borane known to exist in the tetragonal phase from spectroscopy studies.[10,11]

The $Pmn2_1$ orthorhombic unit cell contains two NH_3BH_3 molecules in a nearly body centered arrangement resulting in a layered structure consisting of planes of B−N bonds separated by hydrogen-rich interlayers, as shown in Figure 1a. The B−N bonds of NH_3BH_3 molecule planes are alternately inclined toward the *c*-axis within the mirror plane defined by the *b*- and *c*-axes. Three sets of H···H intermolecular contacts are formed between the amine and the borane hydrogen atoms. The free NH_3BH_3 molecule has C_{3v} symmetry. In the solid phase, the three-fold molecular axes of the amine and borane groups are coincident with the B−N bond and are inclined to the two-fold *c*-axis. The three-fold molecular symmetry is preserved in the orthorhombic space group by placing one hydrogen of each amine or borane group on a special position on the *b*-axis, which is contained in the mirror plane defined by the *b*- and *c*-axes, and another hydrogen in a general position which generates the third hydrogen atom by the mirror plane operation.

The *I*4*mm* tetragonal unit cell is formally body centered and contains two NH_3BH_3 molecules. The B−N bond is aligned parallel to the four-fold *c*-axis, as shown in Figure 1b. The superposition of the C_{3v} molecular symmetry and the four-fold

* To whom correspondence should be addressed. Phone: 509-371-6385. Fax: 509-371-6354. E-mail nancy.hess@pnl.gov.
† Pacific Northwest National Laboratory.
‡ University of Michigan.
§ Los Alamos National Laboratory.

10.1021/jp900839c CCC: $40.75
Published on Web 04/17/2009

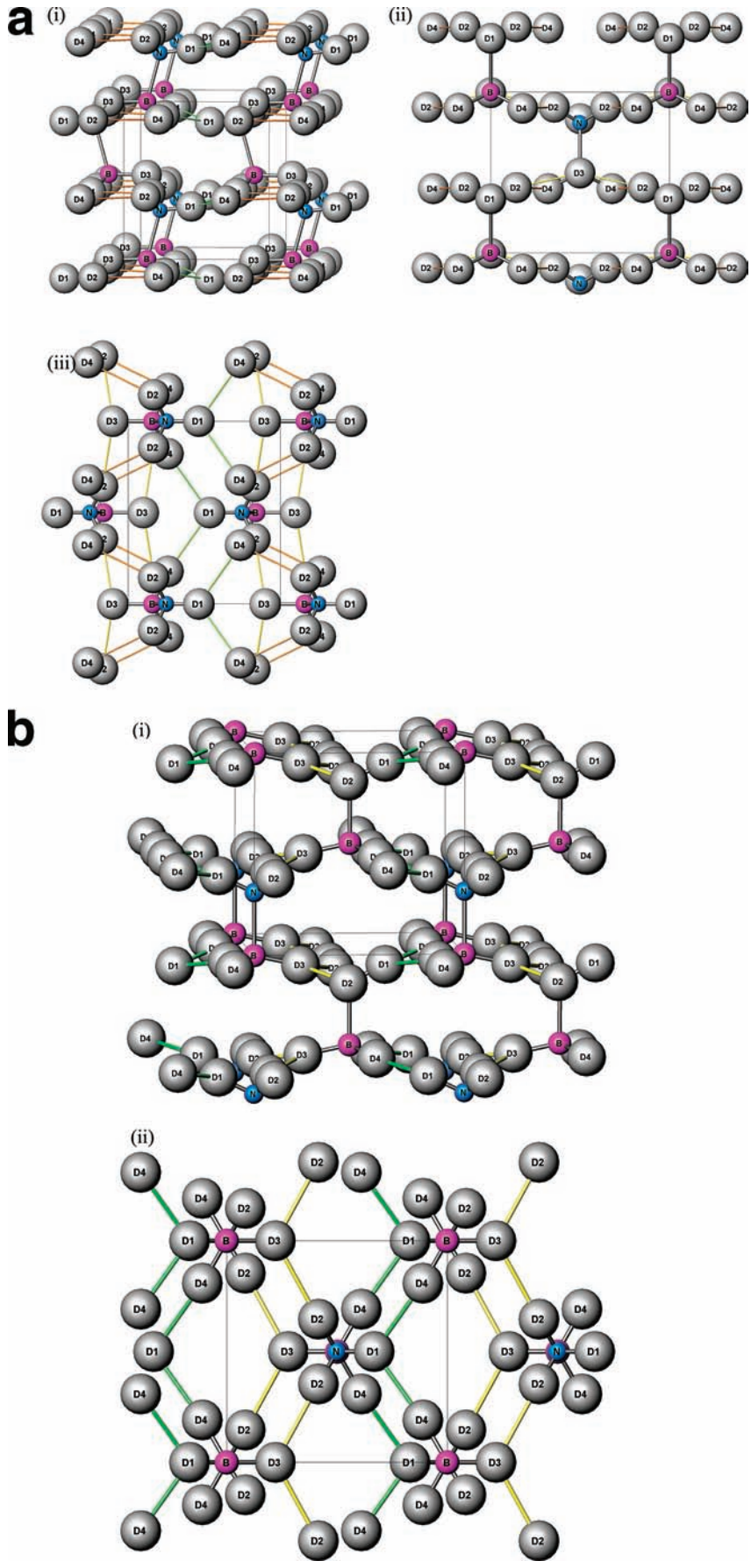

Figure 1. (a) Orthorhombic $Pmn2_1$ crystal structure at 15 K showing the dihydrogen bonding network consisting of three distinct dihydrogen bond sets, D2···D3 yellow, D2···D4 orange, D1···D4 green. (i) View of the $b-c$ plane, (ii) view of the $a-c$ plane, and (iii) view of the $a-b$ plane. (b) One of four possible orientations of the ammonia borane molecule in the tetragonal $I4mm$ crystal structure at 240 K showing the dihydrogen bonding network consisting of two distinct dihydrogen bond sets, D2···D3 yellow and D1···D4 green. (i) View of the $a-c$ plane and (ii) view of the $a-a$ plane.

symmetry requires that the hydrogen atoms are disordered about the B and N atoms in the tetragonal phase.[2,3,9] We chose a 12-site model with 1/4 fractional occupancy to represent the hydrogen disorder rather than the 8-site model with 3/8 occupancy used in recent studies.[8,9] Both models provide an adequate representation of the hydrogen disorder, which is manifested as an annular ring capping the nitrogen and boron atoms; however, the 12-site model is consistent with the spectroscopic results which indicate that the C_{3v} molecular symmetry is preserved in the tetragonal phase.[10−12]

The orthorhombic phase of ammonia borane is structurally similar to the low temperature, ordered phases of ethane (C_2H_6, $P2_1/n$, $Z = 2$),[13] hexachloroethane (C_2Cl_6, *Pnma*, $Z = 4$),[14] and hexabromoethane (C_2Br_6, *Pnma*, $Z = 4$)[15] in that they have their molecular three-fold axis inclined to the two-fold crystallographic *c*-axis within the *b*−*c* plane. Ethane melts at 89 K, whereas C_2Cl_6 and C_2Br_6 transform to higher symmetry, orientationally disordered phases at 318 and 400 K, respectively. They both transform to cubic *Im*3*m* structures where the three-fold molecular axes lie along the body diagonals of the cubic crystallographic cell,[16,17] requiring orientational disorder of the chlorine or bromine atoms. The phase transition to the *Im*3*m* in C_2Cl_6 is thought to involve a two-step transition mechanism and an intermediate monoclinic phase. Temperature-dependent Raman studies of ammonia borane have also suggested the possible existence of an intermediate phase over a narrow temperature range between 215 and 225 K.[10] The results of this NPD structural investigation do not support the existence of symmetrically distinct intermediate phase; however, it does indicate the progressive displacive motions in the orthorhombic phase culminating in an order−disorder phase transition at 225 K.

In this work, we describe the results of a neutron powder diffraction (NPD) study of a ^{2}H-,^{11}B-enriched ammonia borane ($ND_3{}^{11}BD_3$) over the temperature range from 15 to 340 K. We observe orthorhombic and tetragonal structures that are in excellent agreement with earlier work.[2,8,9] The12-site model that we adopt to represent the hydrogen disorder in the tetragonal phase permits description of the dihydrogen bonding network across the temperature range investigated.

Our results from Rietveld refinement are compared to results based on a molecular simulation approach that features the coupling of an electronic structure description of molecular interaction to two statistical sampling methods that provide slightly different perspectives of the ammonia borane structure. We find an excellent correlation between the mean field average and the results from Rietveld refinement, whereas the ensemble average provides a molecular scale representation. Using this approach, we investigate both the internal, intramolecular structure, as well as intermediate range interactions that are most sensitive to intermolecular interactions.

Experimental Section

Synthesis of $ND_3{}^{11}BD_3$. Perdeuterated, ^{11}B-enriched $ND_3{}^{11}BD_3$ polycrystalline powder was synthesized in a multistep processing route described previously.[18,19]

Total Diffraction Experiments. The diffraction experiments were conducted at the LANSCE Lujan center on the NPDF time-of-flight diffractometer[20] on three separate occasions. Approximately 1 g of $ND_3{}^{11}BD_3$ powder was loaded into a vanadium can under He atmosphere. The sample can was attached to a closed-cycle He refrigerator, and temperature was monitored and controlled to ±1 K of the desired temperature. Over the course of the three experimental runs, diffraction data were collected at 15, 100, 120, 175, 220, 230, 240, 275, 330, and 340 K.

The diffracted neutrons were detected on eight symmetrically paired detector banks with 2Θ at 40, 90, 119, and 148° and a cumulative momentum transfer range, *Q*, from 0.8 to 51 Å^{-1}. The detector bank resolution, $\Delta Q/Q$, is 0.51, 0.31, 0.28, and 0.15%, respectively, for the 46, 90, 119, and 148° banks. The powder diffraction data were refined using the Rietveld method[21] and the GSAS program[22] with EXPGUI interface[23] (NIST). For data sets collected below 225 K, refinements were performed in the $Pmn2_1$ space group. The 200 K structure reported by Klooster et al.[2] was used as a starting point for refinements. We use the symbol D for deuterium when referring to the hydrogen atoms in ammonia borane and add the D*n* designation to refer to hydrogen atoms constituting the amine group for $n = 1$ to 2, and for the borane group, $n = 3$ to 4. In the orthorhombic phase, D1 and D3 are the symmetrically unique hydrogen atoms constrained to lie on the *b*-axis. D2 and D4 are hydrogen atoms that sit on general positions. Above 225 K, the structure was refined in the tetragonal *I*4*mm* space group with a 12-site model for the hydrogen positions. Each of 12 sites for the amine and borane hydrogen atoms are symmetrically equivalent, although 4 of the 12 sites sit on special positions and the remaining 8 are on general positions. The 12 sites were constrained to be equivalent by the imposing following relationship, 8*d* site: (0, *y*, *z*) and 16*e* site: ($y\cos(\pi/6)$, $y\sin(\pi/6)$, *z*).

The TOF profile function used was based one developed by David and Von Dreele (unpublished) to describe the leakage of fast and slow neutrons from the moderator. It consists of the Ikeda−Carpenter function convolved with a pseudo-Voight function. The refinement parameters included, in the order refined, the scale factor, zero, background, the unit cell parameters, peak shape function, atomic fractional coordinates, and displacement parameters. A shifted Chebyschev polynomial with 7 to 27 terms was used as the basis for the background function. All atomic displacement parameters were initially treated as isotropic for the initial rounds of refinement and then were allowed to be anisotropic below 220 K. The position of ammonia borane molecule in the $Pmn2_1$ and *I*4*mm* unit cells is translationally invariant along the *c*-axis. Since the boron atom sits near $z = 0$ in earlier refinements,[2,8,9] it was constrained to be at $z = 0$ to make the temperature dependence of the atomic positions discernible from the fractional coordinates. In the tetragonal phase, the atomic displacement parameters for the deuterium atoms were refined using TLS matrices.[24]

The software program PDFgetN was used to extract the experimental pair distribution function extraction from the total diffraction data.[25] For this analysis, only data from the 90, 119, and 148° detector banks were included in the calculation of *S*(*Q*), and furthermore, the intensity of the data from banks 90 and 119° were autoscaled to the 148° bank prior to merging the data banks. The atomic pair distribution function (PDF) is obtained from powder diffraction measurements by making a Fourier transform of the normalized scattering intensity, *S*(*Q*). Explicitly

$$G(r) = 4\pi r[\rho(r) - \rho_0] = \frac{2}{\pi}\int_0^\infty \mathrm{d}Q Q[S(Q) - 1]\sin(Qr)$$

The effective density of the sample was varied until *S*(*Q*) approached unity at the maximum *Q* range, and no attempt was made to account for the presence of hydrogen due to the incomplete deuteration of the sample. The *G*(*r*) was calculated from the *S*(*Q*) over the *Q* range from 1.0 to 20 Å^{-1}.

The software program PDFFIT[26] was used to calculate the *G*(*r*) based on the structure determined by the Rietveld refinement at each temperature. The lattice parameters, fractional coordinates, and isotropic atomic displacement parameters were

used to calculate $G(r)$ but not refined. Only the scale factor and low r sharpening factor were refined over the r range from 5 to 15 Å and 0.5 to 5 Å, respectively. At temperatures greater than 220 K, the low r sharpening factor was fixed at 0.4. Due to the hydrogen background,[19] no attempts were made to fit the calculated $G(r)$ to the experimental data.

Molecular Simulations. The goal of the molecular simulations is to generate an ensemble of configurations corresponding to a canonical ensemble at temperature, T. The volume of the system is fixed, set by the lattice constants determined from neutron diffraction experiments.

To describe the molecular interaction, we used ab initio electronic structure using periodic Density functional theory (DFT) using a PBE functional,[27] Goedecker pseudopotentials, and a TZVP basis set.[28,29] A $2 \times 2 \times 2$ unit cell consisting of 16 ammonia borane molecules was used in the simulation. We assume that all atoms within the unit cell are independent degrees of freedom that are allowed to respond to their neighbors to compose the collective response and energy of the material. This defines a Hamiltonian of the system to perform statistical analysis and to generate ensembles of representative configurations to be used for further, more detailed analysis.

Previous electronic structure analysis of ammonia borane was based on harmonic analysis.[30] Constant temperature dynamics trajectories were generated using the CP2K ab initio molecular simulation package.[31−34] A series of temperatures were simulated. Simulations of 15 000 steps with a time step of 0.5 fs were used to generate configurations. A Nose−Hoover chain ensured proper thermalization of the system. To match the experimental measurements, the simulated temperatures consisted of 15, 100, 120, 175, 220, 230, 240, 275, and 330 K.

The atom-pair radial distribution functions

$$g_{ab}(r) = \frac{V}{4\pi N_a N_b r^2} \sum_R \sum_{i,j} \langle \delta(r - |\mathbf{r}_i - \mathbf{r}_j + \mathbf{R}|) \rangle \delta_{a_i,a} \delta_{a_j,b}$$

were generated from the ensemble of configurations. Here V is the volume of the simulation cell, N_a is the number of atoms of type a in the cell, r_i is the atomic position of atom i, a_i is the atom type of atom i, and $\mathbf{R}$ is a lattice vector. Note that $\sum_i \delta_{a_i,a} = N_a$. Angled brackets denote averages over the statistical ensemble of configurations.

The total neutron scattering pair distribution function (PDF), $G(r)$, is defined as

$$G(r) = \frac{1}{r} \sum_{i,j} \left[\frac{b_i b_j}{\langle b \rangle^2} \delta(r - r_{ij}) \right] - 4\pi r \rho_0$$

where b_i is the coherent neutron scattering length for atom i and ρ_0 is the average atomic density. In terms of the atom pairs

$$G(r) = \frac{4\pi (\sum_a N_a) r}{V (\sum_a N_a b_a)^2} \sum_{a,b} N_a N_b b_a b_b (g_{ab}(r) - 1)$$

where b_a are coherent neutron scattering lengths of atom type a. From the g_{ab} pairs, we are able to identify peaks in the PDF with molecular structure.

To extend the analysis to distances that are beyond the size of the unit cell, we developed a self-consistent procedure. For unlike atom pairs, we consider interaction and correlation with all atoms within the simulation cell as well as all periodic images of a given atom outside the simulation cell. The motion of the atoms outside the simulation cell is perfectly correlated with an image within the simulation cell. For like atom pairs, we assume that each atom is statistically independent with fluctuations determined from a Gaussian distribution of atomic Cartesian positions. The mean position and variance is determined through averaging of the atomic Cartesian coordinates as sampled by the simulation-generated ensemble.

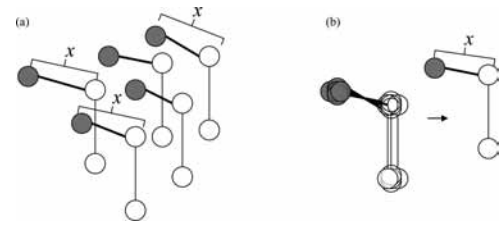

Figure 2. Distinction between the determination of (a) the ensemble $\langle x(\mathbf{r}) \rangle$ and (b) mean field averages $x(\langle (\mathbf{r}) \rangle)$ from molecular dynamic simulations.

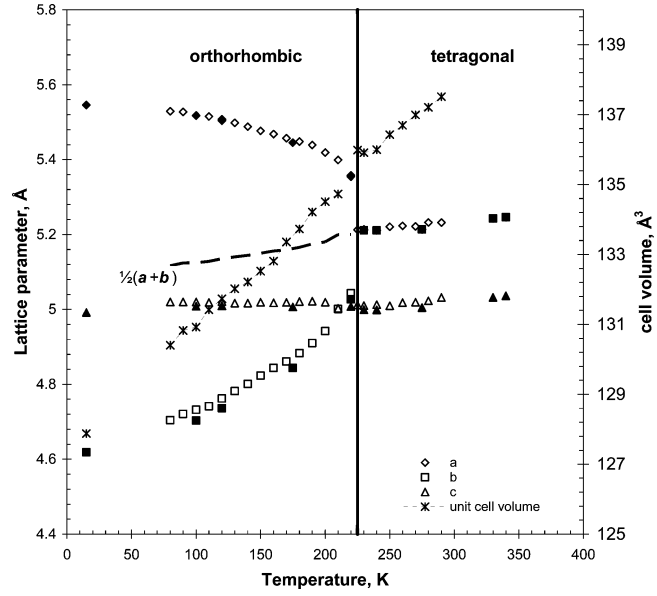

Figure 3. Lattice parameters as a function of temperature. Open symbols are from ref 1; closed symbols are experimental results from this study. Experimental uncertainty is ±0.001 and ±0.0001 Å for the lattice parameters from ref 1 and this study, respectively.

From the ensembles, we have calculated averages of metrical parameters at each temperature by two methods. The *ensemble average* is the average metrical parameter such as bond length calculated directly from each element in the ensemble. The *mean field average* is the metrical parameter calculated from a mean structure representing the average of all the elements in the ensemble. These two averages result in different values and temperature dependencies. An illustration to aide in the distinction between these two averages is given in Figure 2, and a mathematical derivation of the relationship between the two averages is given below:

The relation between the mean field metric, $x(\langle \mathbf{r} \rangle)$ and the ensemble averaged metric, $\langle x(\mathbf{r}) \rangle$, can be seen through the expansion

$$\langle x(\mathbf{r}) \rangle = x(\langle \mathbf{r} \rangle) + \frac{1}{2} \langle \delta\mathbf{r} \delta\mathbf{r} \rangle : \frac{\partial^2 x}{\partial \mathbf{r}\, \partial \mathbf{r}} + \ldots$$

where $\mathbf{r} = \langle \mathbf{r} \rangle + \delta\mathbf{r}$, and $(\partial^2 x)/(\partial \mathbf{r} \partial \mathbf{r})$ is evaluated at $\langle \mathbf{r} \rangle$ where $\mathbf{r}$ represents atomic Cartesian coordinates while x represents metrical parameters. The standard deviation of the ensemble metric, represented by "error bars" in Figures 4 and 5, is $\sigma = \sqrt{\langle x(\mathbf{r})^2 \rangle - \langle x(\mathbf{r}) \rangle^2}$. Expanding this quantity

$$\sigma^2 = \langle x(\mathbf{r})^2\rangle - \langle x(\mathbf{r})\rangle^2 = \langle \delta\mathbf{r}\delta\mathbf{r}\rangle : \frac{\partial x}{\partial \mathbf{r}}\frac{\partial x}{\partial \mathbf{r}} + \ldots$$

If we have a complete set of metric parameters, x_i, to characterize the Cartesian coordinates, and if the Jacobian, $(\partial x_i)/(\partial \mathbf{r})$ is invertable, and correlation between two different x_i is neglected, then we have

$$x(\langle \mathbf{r}\rangle) = \langle x(\mathbf{r})\rangle = \frac{1}{2}\sigma^2 \frac{\partial \mathbf{r}}{\partial x}\frac{\partial \mathbf{r}}{\partial x} : \frac{\partial^2 x}{\partial \mathbf{r}\,\partial \mathbf{r}} + \ldots$$

This indicates that increased thermal fluctuations tend to lower the value of the mean field average. Additionally, in the absence of thermal fluctuations, the two averages have equivalent value. Thus for bond lengths, the mean field average is generally less than the ensemble average at a given temperature and the mean field average shows a stronger temperature dependency.

Results

The results of the Rietveld refinement are compared to the NPD data for 90° 2θ bank at 15, 220, 230, and 340 K in the Supporting Information. The experimental conditions and lattice parameters are listed in Table 1. The refinement results for the fractional coordinates are listed in Table 2, while the anisotropic displacement parameters are given in the Supporting Information. The calculated intramolecular and intermolecular bond lengths and angles are listed in Table 3, and the observed temperature dependence is discussed below and compared to earlier diffraction studies and molecular simulation.

The temperature dependence of the lattice parameters determined from the neutron powder diffraction experiments, shown in Figure 3, are in good agreement X-ray powder diffraction experiments reported by Hoon and Reynhardt.[1] Shown in Figure 3 is a line representing the temperature dependence of the average of a and b lattice parameters in orthorhombic phase, which displays a slightly steeper slope than the a lattice parameter in the tetragonal phase and only a minor discontinuity at the phase transition. Given this relationship and the fact that the c lattice parameter is nearly independent of temperature, unit cell volume increases nearly linearly with increasing temperature over the entire temperature range investigated.

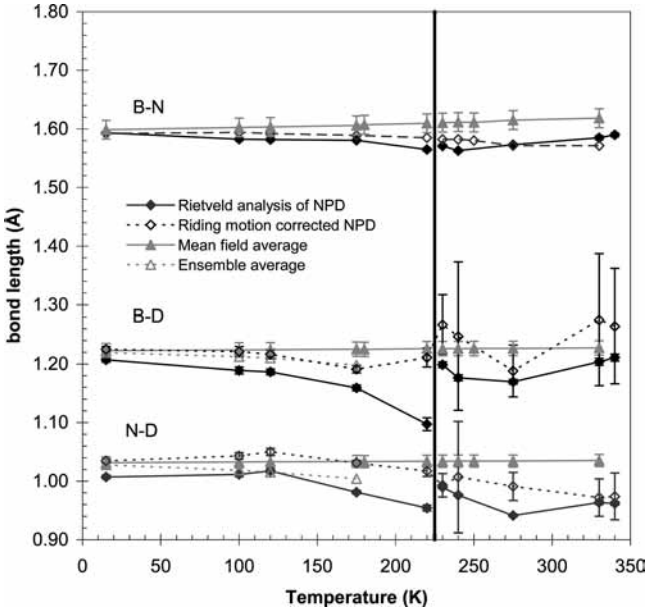

Figure 4. Temperature dependence of the B−N, B−D, and N−D intramolecular bond lengths. The experimentally determined bond lengths from Rietveld analysis of the NPD data and riding motion corrections to these bond lengths are compared to the results of molecular dynamics simulations, specifically the mean field and ensemble averages.

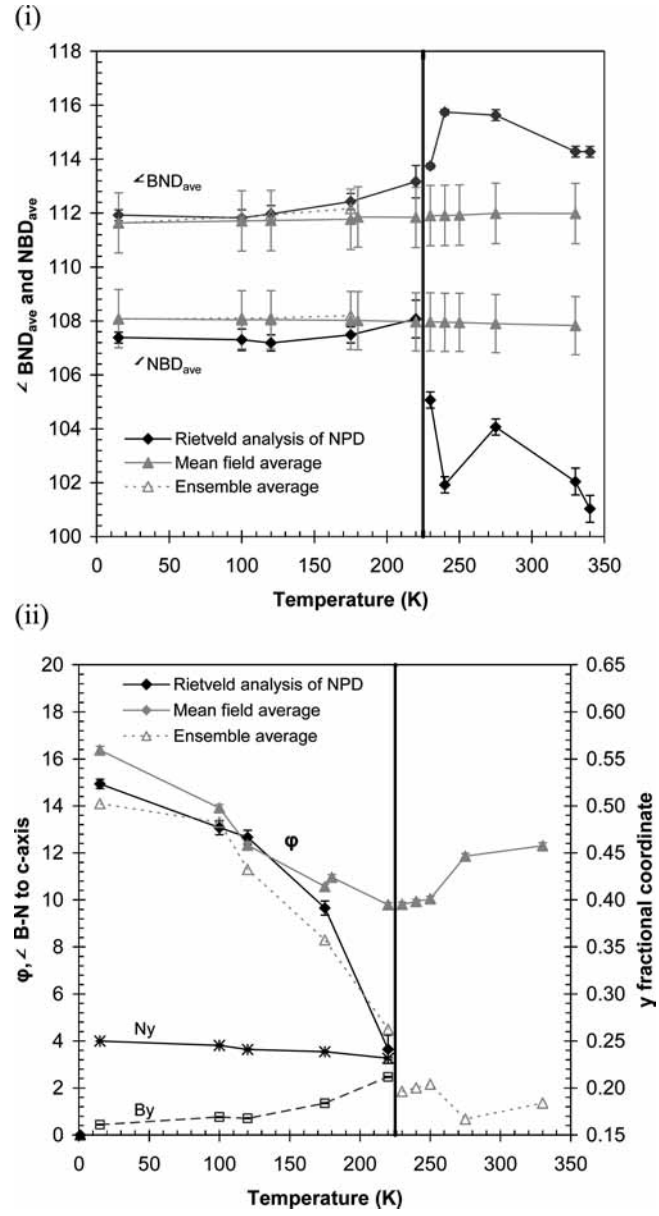

Figure 5. Temperature dependence of the intramolecular bond angles. The experimentally determined bond angles from Rietveld analysis of the NPD data are compared to the results of molecular dynamics simulations, specifically the mean field and ensemble averages. (i) Temperature dependence of the average B−N−D and N−B−D bond angles. (ii) Temperature dependence of φ, the angle of the B−N bond to the c-axis, and the fractional coordinates Ny and By.

Intramolecular Bond Lengths and Angles. The temperature dependencies of the intramolecular B−N and the average B−D and N−D bond lengths[35] between 15 and 340 K are plotted in Figure 4. The numeric values for the individual amine and borane bond lengths are compared to literature values and values from molecular dynamic simulations in Tables 3A and 3B,3C, respectively. In the orthorhombic phase, the B−N bond length decreases by about 0.03 Å with temperature approaching the phase transition boundary. The average B−D and N−D bond lengths decrease by 0.1 and ca. 0.05 Å, respectively, over this temperature range, which is greater than the average standard deviation of ±0.004 Å for these measurements. Additionally,

TABLE 1: Experimental Acquisition Parameters and Refinement Figures of Merit

formula	$ND_3{}^{11}BD_3$				
mass (amu)	37.096				
diffractometer	NPDF at LANSCE				
scan mode	time of flight				
2Θ banks (1−4)	46, 90, 119, 148				
range of *d* spacings (banks 1−4)	1.5−5.1, 0.8−3.75, 0.7−3.0, 0.6−2.6				
absorption coefficient (cm^{-1})	0.0298				
space group $Pmn2_1$, no. 31		temperature (K)			
	15	100	120	175	220
a (Å)	5.54554(9)	5.5175(1)	5.5037(1)	5.44519(13)	5.3544(1)
b (Å)	4.61885(8)	4.7034(1)	4.7361(1)	4.84365(13)	5.0272(1)
c (Å)	4.99168(6)	5.0087(1)	5.00939(5)	5.00643(16)	5.00736(5)
V ($Å^3$)	127.857	129.979	130.576	132.043	134.786
ρ (g cm^{-3})	0.963	0.948	0.944	0.933	0.914
no. of reflections used	820	831	820	729	866
no. of refined parameters[a]	126	126	126	126	126
R_P	0.0104	0.0079	0.0072	0.0068	0.0069
R_{wp}	0.01152	0.0118	0.0108	0.0103	0.0105
$R(F^2)$	0.0770	0.1006	0.1031	0.1324	0.1499
χ^2	2.245	1.410	1.354	1.697	1.321
space group *I4mm*, no. 107		temperature (K)			
	230	240	275	330	340
$a = b$ (Å)	5.2116(9)	5.21088(1)	5.21625(1)	5.24266(6)	5.24618(8)
c (Å)	4.99919(6)	4.99878(1)	5.00449(5)	5.03202(5)	5.03601(5)
V ($Å^3$)	135.784	135.733	136.168	138.308	138.603
ρ (g cm^{-3})	0.907	0.907	0.905	0.890	0.888
no. of reflections used	309	186	300	301	301
no. of refined parameters	92	92	92	92	92
R_P	0.0087	0.0130	0.0066	0.0065	0.0065
R_{wp}	0.0128	0.0195	0.0103	0.0099	0.0097
$R(F^2)$	0.1296	0.1910	0.1667	0.1744	0.1924
χ^2	1.926	1.159	1.833	1.275	1.285

[a] This number includes a total of approximately 79 variables that are used to describe the background in the four detector banks.

TABLE 2: Fractional Coordinates for Ammonia Borane

	temperature (K)									
	15	100	120	175	220	230	240	275	330	340
B/*x*	0	0	0	0	0	0	0	0	0	0
y	0.1610(4)	0.1691(6)	0.1678(6)	0.1839(5)	0.2118(11)	0	0	0	0	0
z	0	0	0	0	0	0.0000(6)	0.0000(25)	0.0000(5)	0.0000(9)	0.0000(10)
N/*x*	0	0	0	0	0	0	0	0	0	0
y	0.2499(3)	0.2453(5)	0.2410(5)	0.2386(4)	0.2316(7)	0	0	0	0	0
z	0.3084(3)	0.3078(5)	0.3081(3)	0.3112(3)	0.3119(3)	0.3142(0)	0.3127(24)	0.3143(0)	0.3150(0)	0.3157(0)
D1/*x*	0	0	0	0	0	0	0	0	0	0
y	0.4650(5)	0.4561(8)	0.4482(9)	0.4315(6)	0.4104(14)	0.1738(32)	0.169(7)	0.163(4)	0.168(5)	0.167(6)
z	0.3347(6)	0.3378(6)	0.3408(10)	0.3516(7)	0.3796(18)	0.3939(26)	0.397(7)	0.3957(30)	0.394(4)	0.394(5)
D2/*x*	0.1443(3)	0.1459(4)	0.1498(4)	0.1445(4)	0.1415(6)	0.1505(18)	0.146(4)	0.1409(24)	0.1451(29)	0.145(4)
y	0.1681(4)	0.1619(6)	0.1598(5)	0.1562(5)	0.1481(9)	0.0869(13)	0.0843(23)	0.0813(13)	0.0838(20)	0.0836(22)
z	0.4058(4)	0.4035(4)	0.4037(5)	0.4026(4)	0.3904(12)	0.3939(14)	0.3975(0)	0.3957(15)	0.3937(21)	0.3942(23)
D3/*x*	0	0	0	0	0	0	0	0	0	0
y	−0.1013(7)	−0.0792(12)	−0.0776(9)	−0.0557(9)	0.0018(25)	0.222(8)	0.221(14)	0.217(7)	0.225(17)	0.227(15)
z	−0.0079(8)	−0.0155(10)	−0.0165(11)	−0.0266(8)	−0.0559(22)	−0.062(7)	−0.049(13)	−0.057(5)	−0.050(14)	−0.046(12)
D4/*x*	0.1790(3)	0.1787(7)	0.1775(7)	0.1762(5)	0.1830(14)	0.192(5)	0.191(9)	0.188(4)	0.194(12)	0.196(10)
y	0.2610(5)	0.2714(8)	0.2732(9)	0.2800(7)	0.32806(20)	0.1110(27)	0.110(5)	0.1088(25)	0.112(5)	0.113(5)
z	−0.1005(4)	−0.0962(8)	−0.0957(10)	−0.0886(6)	−0.0719(5)	−0.062(4)	−0.049(8)	−0.0568(30)	−0.050(8)	−0.046(7)

at any given temperature, we found only minor differences between the N−D1 and N−D2 bond lengths and similarly for the B−D3 and B−D4 bond lengths. The similar bond length for symmetrically distinct hydrogen atoms would be expected due to the C_{3v} molecular symmetry but is not guaranteed by Rietveld refinement in the $Pmn2_1$ orthorhombic space group.

At low temperature, while our structure is in general agreement with earlier studies, there are discrepancies in the intramolecular bond lengths. At 15 K, our value for the B−N bond length, 1.593 Å, is significantly longer than the 1.573 Å determined from neutron studies at 16 K[8] and in agreement, within experimental uncertainty, with the 1.599 Å measured in single-crystal X-ray studies at 90 K.[9] The N−D and B−D bond lengths determined in this study are in better agreement with the neutron study and approximately 0.1 Å longer than those determined in the single-crystal X-ray studies. The approximately +0.1 Å discrepancy between neutron and X-ray bond length determinations is typical and is attributed to the measurement of internuclear distance in neutron studies versus interelectronic distances in X-ray studies.

At 175 K, our bond length determinations are in good agreement with earlier measurements[2] at 200 K within experimental uncertainty. However, our 220 K determinations of the B−N, B−D*n*, and N−D*n* bond lengths are about 0.015, 0.05, and 0.05 Å shorter, respectively, than those determined by Klooster et al. at 200 K[2] and may reflect the proximity of the 220 K measurement to the

TABLE 3A: Bond Lengths and Angles for Ammonia Borane and Comparison with Literature Values (Literature Values Are in Bold Font)

	temperature (K)							
	15	16[a]	90[b]	100	120	175	200[c]	220
B−N	1.593(2)	**1.579**	**1.599(8)**	1.583(3)	1.582(3)	1.581(2)	**1.58(2)**	1.565(4)
B−D3	1.212(4)	**1.210**	**1.13(4)**	1.171(6)	1.165(5)	1.168(5)	**1.15(5)**	1.092(5)
B−D4	1.205(2)	**1.222**	**1.08(5)**	1.198(4)	1.197(4)	1.155(3)	**1.18(3)**	1.100(4)
N−D1	1.002(3)	**0.972**	**0.80(6)**	1.003(4)	0.995(4)	0.956(3)	**1.07(4)**	0.961(4)
N−D2	1.010(2)	**1.012**	**0.96(4)**	1.016(2)	1.028(2)	0.994(2)	**0.96(3)**	0.951(2)
φ	14.9(2)	**15.5**	**13.1**	13.1(3)	12.7(3)	9.7(3)	**8.87**	3.7(5)
D1−N−B	112.5(2)	**114.1**	**111(6)**	111.7(3)	112.2(3)	111.9(3)	**106(4)**	114.3(4)
D2−N−B	111.6(1)	**111.5**	**110(2)**	111.9(2)	111.9(2)	112.7(2)	**111(2)**	112.6(7)
D3−B−N	106.8(2)	**106.5**	**105(4)**	106.9(4)	106.7(3)	106.2(3)	**114(2)**	108.5(6)
D4−B−N	107.7(2)	**105.6**	**106(2)**	107.5(3)	107.4(3)	108.1(3)	**112(1)**	107.9(7)
D1-N−D2	107.0(1)	**105.8**	**109**	108.1(3)	107.0(3)	107.2(2)	**113(3)**	105.5(5)
D2−N−D2	104.8(3)	**107.8**	**109**	104.8(4)	106.6(4)	104.7(3)	**104(3)**	105.6(6)
D3−B−D4	111.7(2)	**114.4**	**117**	112.0(4)	112.8(3)	110.9(3)	**102(2)**	102.7(6)
D4−B−D4	111.0(3)	**109.5**	**106**	110.7(5)	109.4(5)	112.3(5)	**115(3)**	126(1)
	intermolecular bond lengths and angles							
D1···D4	2.208(3)	**2.213**	**2.45**	2.212(5)	2.234(5)	2.270(4)	**2.21(4)**	2.313(8)
D2···D3	2.043(4)	**2.040**	**2.10**	2.033(4)	2.006(4)	2.027(4)	**2.02(3)**	2.080(6)
D2···D4	2.211(4)	**2.246**	**2.37**	2.256(4)	2.260(5)	2.328(4)	**2.22(4)**	2.359(7)
N−D1···D4	126.0(3)	**126.2**	**128**	126.5(4)	127.3(4)	129.0(3)	**129.6**	131.7(6)
N−D2···D3	157.4(2)	**159.9**	**163**	158.4(3)	159.3(3)	158.9(3)	**156.1**	161.5(5)
N−D2···D4	132.8(2)	**131.5**	**138**	133.6(3)	132.6(3)	134.9(3)	**137.5**	138.9(5)
D1···D4−B	161.0(3)	**163.7**	**165**	162.2(3)	162.1(4)	160.8(3)	**155.6**	154.1(6)
D2···D3−B	99.1(2)	**98.8**	**104**	101.5(4)	101.7(3)	105.1(3)	**105.5**	112.4(7)
D2···D4−B	90.9(2)	**88.4**	**90**	89.5(3)	88.0(4)	89.4(3)	**93.8**	95.4(6)

	temperature (K)						
	230	240	275	295[d]	298[e]	330	340
B−N	1.571(3)	1.563(5)	1.573(2)	**1.656**	**1.597(3)**	1.585(5)	1.590(5)
B−D	1.199(21)	1.177(40)	1.170(17)	**1.204**	**1.11(4)**	1.20(4)	1.21(6)
N−D	0.989(8)	0.976(16)	0.941(10)	**0.936**	**0.85(7)**	0.964(13)	0.962(16)
D−N−B	113.7(9)	115.7(17)	115.6(5)	**110.4**	**114(3)**	114.3(7)	114.3(16)
D−B−N	105.1(11)	101.9(18)	104.1(8)	**99.0**	**110(2)**	102.0(20)	101.0(18)
D−N−D	104.9(4)	102.5(9)	102.7(6)	**83.0**	**81**	104.3(14)	104.3(9)
D−B−D	113.5(12)	115.9(21)	114.3(11)	**88.6**	**82.4**	115.8(26)	116.4(22)
	intermolecular bond lengths and angles						
D1···D4	1.97(2)	2.00(4)	2.03(2)			2.00(3)	1.99(3)
D2···D3	2.09(2)	2.12(3)	2.16(2)	**1.667**	**1.91**	2.13(4)	2.14(4)
D2···D4	2.86(2)	2.88(3)	2.90(2)			2.91(4)	2.92(3)
N−D1···D4	124.5(10)	125.3(19)	125.5(8)			125.9(15)	126.2(15)
N−D2···D3	162.2(8)	161.5(12)	160.7(9)	**171**	**163**	163.3(13)	163.7(13)
N−D2···D4	134.0(9)	134.3(16)	134.6(8)			134.6(17)	134.6(14)
D1···D4−B	170.0(11)	173.1(20)	170.4(8)			173.1(16)	173.8(16)
D2···D3−B	119.2(8)	119.6(12)	119.9(10)	**176**	**168**	119.2(14)	119.0(13)
D2···D4−B	78.4(10)	78.6(16)	79.5(8)			78.4(17)	78.2(15)

[a] Reference 8. [b] Reference 9. [c] Reference 2. [d] Reference 8. [e] Reference 9.

phase transition temperature. At the phase transition boundary, the B−N bond length shows little change, whereas the average N−D and B−D bond lengths increase in length by 0.03 and 0.1 Å, respectively. In the tetragonal phase with increasing temperature, the N−D and B−D lengths change by −0.03 and +0.01 Å, respectively, after passing through minimum values at 275 K. After passing a minimum value at 240 K, the B−N bond length increases by 0.02 Å with increasing temperature. Comparing our 275 K structure and the published values at 298 K, the largest discrepancy is our 1.573 Å determination of the B−N bond length, which is 0.09 Å shorter than that determined in the neutron study[8] but in good agreement with the single-crystal X-ray study.[9]

The observed trend of decreasing bond length with increasing temperature is atypical since it suggests an increase in bond strength with increasing temperature but can result when the thermal motion of an atom pair leads to an apparent shortening of corresponding bond length.[36,37] In ammonia borane, the thermal motion would have an additional contribution from the rotation of the amine and borane groups about the B−N bond. To correct for the apparent shortening, a riding motion correction was applied to the individual N−D*n* and B−D*n* bond lengths using the formulation of Busing and Levy.[36] The corrected bond lengths are shown graphically in Figure 4 and listed in Table 2. The magnitude of the riding motion correction is larger at higher temperature, and the corrected bond lengths are nearly independent of temperature. Note that the riding motion corrected bond length has greater associated uncertainty than the corresponding Rietveld determination because the corrected bond length implicitly includes the uncertainty associated with atomic displacement parameters, whereas this uncertainty is not included in the Rietveld determination. This is especially evident in the tetragonal phase where the riding motion correction is problematic because the atomic displacement parameters used in the calculation are based on the 12-site model with fractional occupancy resulting in nearly an order of magnitude increase in the uncertainty of the corrected value. Nonetheless, within the uncertainty of the correction, no temperature dependence of N−D*n* and B−D*n* bond length is observed.

TABLE 3B: Bond Lengths and Angles for Ammonia Borane: Comparison of Reitveld Analysis of NPD Data with Molecular Dynamic Simulation in Orthorhombic Phase, $x(\langle \mathbf{r} \rangle)$, the Mean Field Average, and $\langle x(\mathbf{r}) \rangle$, the Ensemble Average[a]

	temperature (K)								
	15			100			120		
	NPD	$x(\langle \mathbf{r} \rangle)$	$\langle x(\mathbf{r}) \rangle$	NPD	$x(\langle \mathbf{r} \rangle)$	$\langle x(\mathbf{r}) \rangle$	NPD	$x(\langle \mathbf{r} \rangle)$	$\langle x(\mathbf{r}) \rangle$
B−N	1.593(2)	1.592	1.598(8)	1.583(3)	1.594	1.60(2)	1.582(3)	1.592	1.60(2)
B−D3	1.212(4) *1.230(4)*	1.222	1.22(2)	1.171(6) *1.196(6)*	1.217	1.22(2)	1.165(5) *1.192(5)*	1.215	1.22(2)
B−D4	1.205(2) *1.223(2)*	1.218	1.22(2)	1.198(4) *1.234(4)*	1.21	1.22(2)	1.197(4) *1.229(4)*	1.208	1.22(2)
N−D1	1.002(3) *1.028(3)*	1.023	1.031(6)	1.003(4) *1.041(4)*	1.014	1.03(2)	0.995(4) *1.041(5)*	1.01	1.03(2)
N−D2	1.010(2) *1.038(2)*	1.03	1.031(6)	1.016(2) *1.044(3)*	1.021	1.03(2)	1.028(2) *1.055(3)*	1.018	1.03(2)
φ	14.9(2)	14.1		13.1(3)	13.3		12.7(3)	11.3	
D1−N−B	112.5(2)	112.5	112(1)	111.7(3)	112.8	112(3)	112.2(3)	112.8	112(3)
D2−N−B	111.6(1)	111.2	112(1)	111.9(2)	111.4	112(3)	111.9(2)	111.5	112(3)
D3−B−N	106.8(2)	107.4	108(1)	106.9(4)	107.5	108(3)	106.7(3)	107.5	108(3)
D4−B−N	107.7(2)	108.4	108(1)	107.5(3)	108.4	108(3)	107.4(3)	108.4	108(3)
D1···D4	2.208(3)	2.22		2.212(5)	2.22		2.234(5)	2.22	
D2···D3	2.043(4)	1.99		2.033(4)	2		2.006(4)	1.99	
D2···D4	2.211(4)	2.14		2.256(4)	2.2		2.260(5)	2.23	
N−D1···D4	126.0(3)	127		126.5(4)	127		127.3(4)	128	
N−D2···D3	157.4(2)	157		158.4(3)	158		159.3(3)	157	
N−D2···D4	132.8(2)	132		133.6(3)	132		132.6(3)	133	
D1···D4−B	161.0(3)	159		162.2(3)	159		162.1(4)	160	
D2···D3−B	99.1(2)	97		101.5(4)	100		101.7(3)	100	
D2···D4-B	90.9(2)	90		89.5(3)	90		88.0(4)	89	

	temperature (K)					
	175			220		
	NPD	$x(\langle \mathbf{r} \rangle)$	$\langle x(\mathbf{r}) \rangle$	NPD	$\langle \mathbf{r} \rangle$	ave $\langle \mathbf{r} \rangle$
B−N	1.581(2)	1.589	1.61(3)	1.565(4)	1.585	1.61(4)
B−D3	1.168(5) *1.190(5)*	1.204	1.23(3)	1.092(5) *1.10(1)*		1.23(3)
B−D4	1.155(3) *1.192(3)*	1.195	1.23(3)	1.100(4) *1.268(6)*		1.23(3)
N−D1	0.956(3) *1.015(3)*	0.999	1.03(2)	0.961(4) *1.069(7)*		1.03(2)
N−D2	0.994(2) *1.039(2)*	1.007	1.03(2)	0.951(2) *0.992(4)*		1.03(2)
φ	9.7(3)	8.3		3.65	4.5	
D1−N−B	111.9(3)	113.1	112(4)	114.3(4)		112(4)
D2−N−B	112.7(2)	111.7	112(4)	112.6(7)		112(4)
D3−B−N	106.2(3)	107.8	108(4)	108.5(6)		108(4)
D4−B−N	108.1(3)	108.4	108(4)	107.9(7)		108(4)
D1···D4	2.270(4)	2.22		2.213(8)		
D2···D3	2.027(4)	1.98		2.080(6)		
D2···D4	2.328(4)	2.3		2.359(7)		
N−D1···D4	129.0(3)	130		131.7(6)		
N−D2···D3	158.9(3)	158		161.5(5)		
N−D2···D4	134.9(3)	135		138.9(5)		
D1···D4−B	160.8(3)	160		154.1(6)		
D2···D3−B	105.1(3)	103		112.4(7)		
D2···D4−B	89.4(3)	87		95.4(6)		

[a] Values in italics are corrected for riding motion as described in text.

Average bond lengths calculated by molecular simulation are compared to values from Rietveld analysis in Figure 4 and in Table 2. There is remarkable agreement across the temperature range investigated. The most striking feature is the contrasting temperature-dependent trends presented by the ensemble and mean field averages. This is perhaps most notable for the temperature dependence of the B−N bond length; the ensemble average increases, whereas the mean field average decreases. Additionally, in the orthorhombic phase, the ensemble average for the N−D*n* and B−D*n* bond lengths exhibits no temperature dependence, whereas the mean field average displays decreases in N−D*n* and B−D*n* bond lengths with increasing temperature. Note that disorder in the tetragonal phase prohibits calculation of the mean field average N−D*n* and B−D*n* bond lengths because the hydrogen atoms are no longer uniquely defined. In general, the temperature trends for the uncorrected Rietveld bond lengths follow those exhibited by the mean field average, and the corrected bond lengths follow those displayed by the ensemble average.

The temperature dependences of the average intramolecular ∠BND and ∠NBD angles are shown in Figure 5i. Within the orthorhombic phase, the average ∠BND and ∠NBD angle range from about 111 to 112° and 106 to 108°, respectively, with ±0.3° average uncertainty, and show little temperature dependence. These values are consistent with the recent neutron[8] and X-ray determinations[9] and contradict earlier work.[2] At the 225 K phase transition, the average ∠BND angle changes nearly continuously, whereas the ∠NBD angle decreases by 3.0°. In the tetragonal phase with increasing temperature, the ∠BND angle increases slightly and the ∠NBD angle decreases by 4.0°.

There is excellent agreement between the calculated average ∠BND angle from Rietveld refinement and molecular simulation as seen in Figure 5i and Table 3B, although the statistical uncertainty from ensemble average is quite large. For the corresponding ∠NBD average angle, the magnitude of the Rietveld angle is approximately 1° less than the simulation. Analogous to bond length determined by molecular simulation, the ensemble average bond angles exhibit little temperature dependence and no discontinuity at the phase transition.

Shown in Figure 5ii is the temperature dependence of the angle φ defined as the angle between the B−N bond in the

TABLE 3C: Bond Lengths and Angles for Ammonia Borane: Comparison with Molecular Dynamic Simulation, $\langle x(\mathbf{r})\rangle$, the Ensemble Average in Tetragonal Phase[a]

	temperature (K)							
	230		240		275		330	
	NPD	$\langle x(\mathbf{r})\rangle$	NPD	$\langle x(\mathbf{r})\rangle$	NPD	$\langle x(\mathbf{r})\rangle$	NPD	$\langle x(\mathbf{r})\rangle$
B−N	1.571(3)	1.598(8)	1.563(5)	1.60(2)	1.573(2)	1.60(2)	1.585(5)	1.61(3)
B−D	1.20(2)	1.22(2)	1.17(4)	1.22(2)	1.17(2)	1.22(2)	1.20(4)	1.23(3)
	1.27(5)		*1.2(1)*		*1.19(4)*		*1.27(1)*	
N−D	0.989(8)	1.031(6)	0.98(2)	1.03(2)	0.94(1)	1.03(2)	0.96(1)	1.03(2)
	0.99(2)		*1.01(9)*		*0.99(2)*		*0.97(3)*	
φ	0	10(5)	0	10(5)	0	12(6)	0	12(6)
D−N−B	113.7(9)	112(1)	116(1)	112(3)	115.6(5)	112(3)	114.3(7)	112(4)
D−B−N	105(1)	108(1)	102(2)	108(3)	104.1(8)	108(3)	102(2)	108(4)
D1···D4	1.97(2)		2.00(4)		2.03(2)		2.00(3)	
D2···D3	2.09(2)		2.12(3)		2.16(2)		2.13(4)	
D2···D4	2.86(2)		2.88(3)		2.90(2)		2.91(4)	
N−D1···D4	125(1)		125(2)		125.5(8)		126(2)	
N−D2···D3	162.2(8)		162(1)		160.7(9)		163(1)	
N−D2···D4	134.0(9)		134(2)		134.6(8)		135(2)	
D1···D4−B	170(1)		173(2)		170.4(8)		173(2)	
D2···D3−B	119.2(8)		120(1)		120(1)		119(1)	
D2···D4−B	78(1)		79(1)		79.5(8)		78(2)	

[a] Values in italics are corrected for riding motion as described in text.

b−*c* plane and the *c*-axis. In the orthorhombic phase, we observe a progressive rotation of the B−N bond parallel to the *c*-axis is observed with increasing temperature that is completed at the 225 K transition temperature. As can be seen from comparison of the temperature dependence of the *y* fractional coordinates of the B and N atoms shown in Figure 5ii, the rotation of the B−N bond results from the displacement of the B atom along the *b*-axis until it is sits below N atom.

The rotation of the B−N bond parallel to the *c*-axis is also observed in the molecular simulation. The mean field and ensemble averages are in excellent agreement with the results of Rietveld refinement in the orthorhombic phase. In the Rietveld refinement, symmetry dictates that φ will have zero value in the tetragonal phase. However, the molecular simulations are not constrained by symmetry and suggest that φ does not attain zero value and dynamically that the ammonia borane molecule precesses about the *c*-axis in the tetragonal phase. Interestingly, the ensemble average for φ attains a minimum value of 10° at the phase transition but then continues to increase with increasing temperature, and the ensemble average for the B−N bond length also displays a complementary trend. In contrast, the mean field average value for φ is less than 2° in the tetragonal phase, and the corresponding B−N bond length decreases slightly in tetragonal phase.

Analysis of the molecular dynamic simulations above suggest that it is likely that the apparent shortening of the B−N bond with increasing temperature indicated from Rietveld refinement does not represent the actual geometric state of ammonia borane. The precession of the ammonia borane molecule may lead to the apparent shortening of the B−N bond. In general, the comparison of Rietveld and simulation results suggest that the bond lengths from the Rietveld refinement may be biased toward shorter values due to precession and thermal motion both of which become increasingly important at high temperature.

The above analysis indicates that the intramolecular geometry of the ammonia borane molecule stays intact over the temperature interval investigated and across the phase transition boundary while the unit cell volume increases. Our conceptual model of the low temperature evolution of the orthorhombic structure involves pivoting of the ammonia borane molecule about the N atom rotating the B−N bond parallel to the *c*-axis. Concurrently, the lattice is expanding along *b*-axis and contracting along the *a*-axis, resulting in changes in the intermolecular bond distances and bond angles which define the dihydrogen bonding network. These changes are analyzed in the following section.

Intermolecular Bond Lengths and Angles. In orthorhombic ammonia borane, three potential dihydrogen bonds can be described with one being significantly shorter than the other two (see Figure 1 and insets in Figure 6). The shortest dihydrogen bond is approximately 2.02 Å long and is formed between the D2 of the amine group and D3 of the borane group lying nearly parallel to the *a*-axis. This dihydrogen bond forms a corrugated plane of linked ammonia borane molecules along the *a*−*c* plane. The two longer dihydrogen bonds lengths are both approximately 2.2 Å long and are formed between the amine D1 and borane D4 and between amine D2 and borane D4. The D2···D4 dihydrogen bond also links adjacent ammonia borane molecules together in the corrugated plane. The D1···D4 dihydrogen bond knits the parallel corrugated planes of ammonia borane molecules together in the *b* direction. The temperature dependence of these dihydrogen bonds is shown graphically in Figure 6 and compared to values calculated from the literature[2,8,9] in Table 2. In the orthorhombic phase, our values for the dihydrogen bond lengths and angles are in good agreement with the neutron studies at 16[8] and 200 K[2] but in lesser agreement with the X-ray study at 90 K.[9]

In the orthorhombic phase, all three dihydrogen bonds lengthen with increasing temperature.[38] The shortest dihydrogen bond, D2···D3, displays the weakest temperature dependence. Just below the phase transition, the D1···D4 and D2···D4 dihydrogen bond lengths approach 2.4 Å, the sum of the van der Waals radii for two hydrogen atoms. To extended our analysis of the temperature evolution of the dihydrogen bonding network into tetragonal phase, using the 12-site model for hydrogen disorder, we consider a subset of the four possible orientations of the ammonia borane molecule as a local description of the structure, realizing that the true structure is orientationally disordered occupying all four possible orientations on the longer length scale probed by diffraction. For convenience, this orientational relationship between the orthorhombic and tetragonal phase is shown as insets in Figure 6. D2···D3, the shortest dihydrogen bond in the orthorhombic

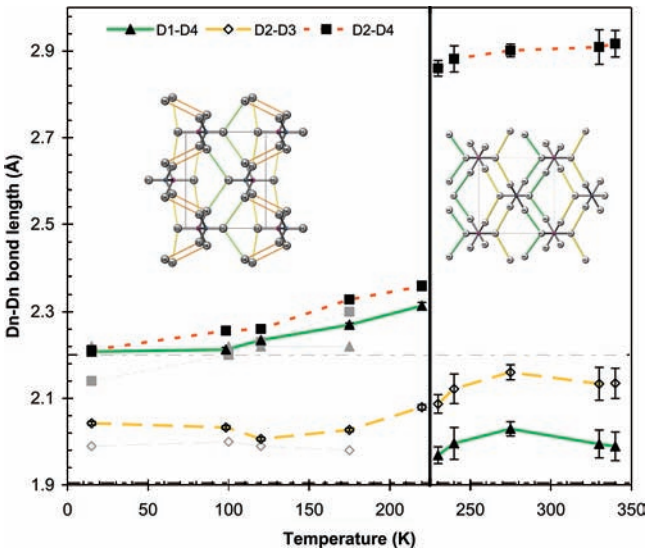

Figure 6. Intermolecular dihydrogen bond lengths as a function of temperature. The mean field average calculated from molecular dynamic simulations is represented by gray symbols. Insets show the distinct dihydrogen bonds that form the dihydrogen bonding network in the orthorhombic and tetragonal phases. The dot-dash lines shows the upper and lower bounds for the majority of B−H···H−N bond lengths found by Klooster et al.[2]

phase, increases nearly continuously across the phase transition boundary, whereas the D1···D4 dihydrogen bond decreases by 0.3 Å and becomes the shortest dihydrogen bond in the tetragonal phase. The D2···D4 dihydrogen bond, which was 2.36 Å at 220 K, becomes 2.860 Å at 230 K and clearly can no longer be considered a dihydrogen bond. In the tetragonal phase, both the D1···D4 and D2···D3 dihydrogen bond lengths increase slightly with increasing temperature.

In a review of dihydrogen bonded molecular materials, Klooster et al. analyzed N−H···H−B intermolecular dihydrogen bond angles in detail and found that the ∠NH···H, ψ, are more linear whereas the ∠BH···H, θ, are more bent.[2] The temperature dependencies of the θ and ψ bond angles in ammonia borane are shown in Figure 7. In the orthorhombic phase, the θ and ψ values determined in this study are in good agreement with Klooster's determination at 200 K[2] and the neutron and X-ray determinations at 16[8] and 90 K,[9] respectively.

In the orthorhombic phase, the ψ angle ∠ND2···D3 increases weakly with increasing temperature and changes nearly continuously at the phase transition boundary. The θ angle ∠BD3···D2 displays the largest temperature dependence increasing from 99° at 15 K to 112° at 220 K, increasing to 119° at the phase transition boundary, and then becoming insensitive to temperature in the tetragonal phase.

The θ and ψ angles associated with the D1···D4 dihydrogen bond have the reversed angular relationship from those expected based on Klooster et al. analysis.[2] The ψ angle ∠ND1···D4 is more bent compared to the θ angle ∠BD4···D1, which is nearly linear. Klooster et al. suggest that D1···D4 may be a weaker dihydrogen bond based on its angular geometry. Theoretical calculations in the gas phase of the angular of sp^3 hybridization of the amine and borane molecular groups support this hypothesis.[39] Since the D1···D4 dihydrogen bond length is the shortest in the tetragonal phase, it would normally be considered the strongest. However, the improbable intermolecular geometry suggests that this bond set is not viable in the orthorhombic or tetragonal phase.

The θ and ψ angles associated with the D2···D4 dihydrogen bond have the predicted angular relationship, with the ψ angle

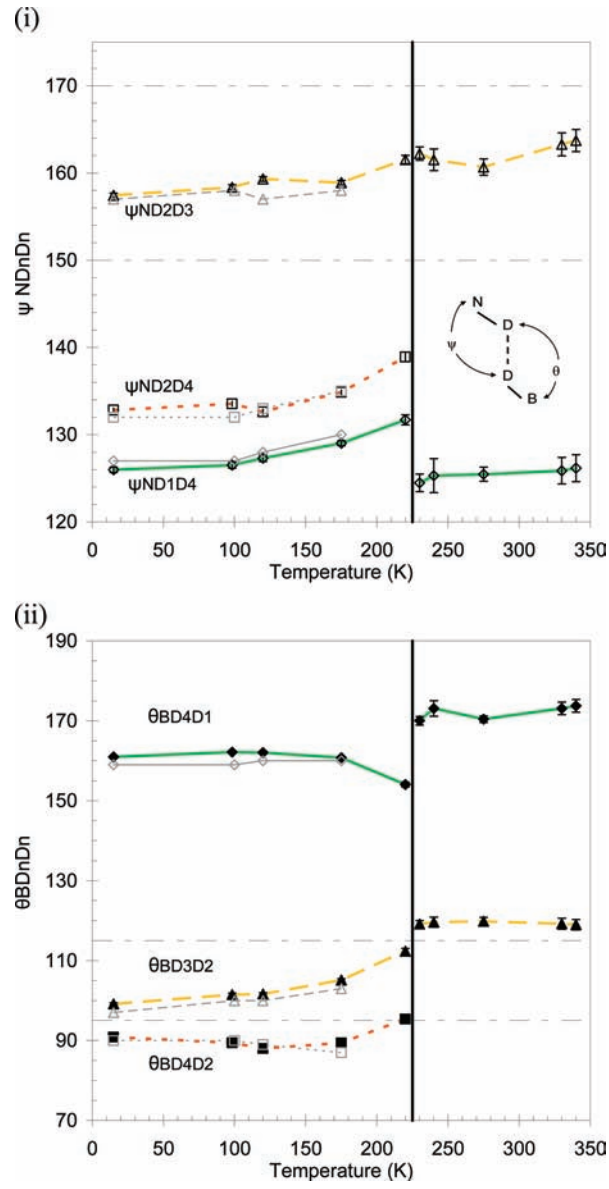

Figure 7. Intermolecular dihydrogen bond angles, ψ (i) and θ (ii), as a function of temperature. Solid green line = D1···D4, dashed yellow line = D2···D3, dotted orange line D2···D4. The gray symbols represent the mean field average calculated from molecular dynamic simulations. Inset shows the definition of the ψ and θ angles adopted from Klooster et al.[2] The dot-dash lines shows the upper and lower bounds for the majority of ψ and θ angles found by Klooster et al.[2]

∠ND2···D4 being more linear, at ca. 134°, and the θ angle ∠BD4···D2 near 90 ° in the orthorhombic phase. In the tetragonal phase, the length of this dihydrogen bond is becomes nearly 2.9 Å in the tetragonal phase and is too long to be considered a dihydrogen bond.

The above analysis of the molecular geometry of the ammonia borane dihydrogen bonding network suggests that only one of the three possible dihydrogen bonds, D2···D3, persists across the phase transition and only D2···D3 and D2···D4 are viable dihydrogen bonds in the orthorhombic phase. Metrical parameters for the dihydrogen bonding network based on the molecular dynamics simulation can only be calculated for the mean field average in the orthorhombic phase. The mean field average is compared to the results of Rietveld refinement in Figures 6 and 7. Both the numerical values and temperature trends are in remarkable agreement for both dihydrogen bond length and bond angles.

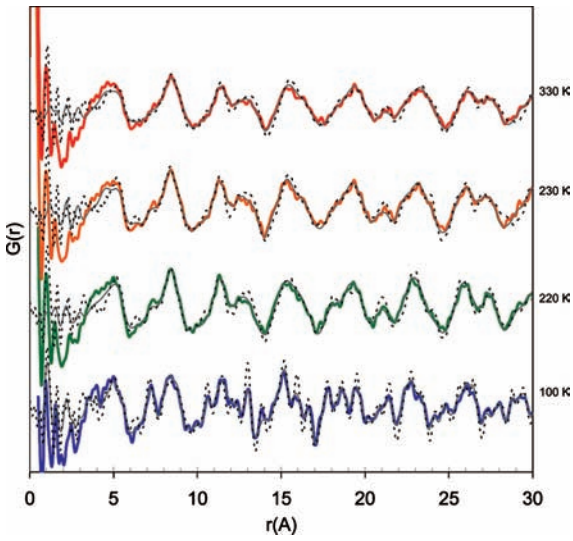

Figure 8. Experimental pair distribution function extracted from total diffraction data at temperatures above and below the structural phase transition at 225 K compared to $G(r)$ calculated from Rietveld structure (gray lines) and calculated from ensemble average from simulation (black dashed line) over the radial distance from 0 to 30 Å (a). $Q_{max} = 20$ Å^{-1}.

PDF Analysis. The experimental pair distribution function (PDF) at temperatures above and below the phase transition is compared to a calculated PDF based on the structure from Rietveld refinement and the PDF calculated from the molecular dynamics simulation in Figure 8. At radial distances greater than 5 Å, the agreement between the experimental and both calculated PDFs is remarkable for matching both the amplitude and the radial structure. Since agreement will only result if Rietveld refinement and the molecular dynamics simulation accurately represent the long-length scale structure of ammonia borane, the excellent agreement validates the refined and simulated structures. Below 5 Å, the magnitude of the $G(r)$ experimental curve is less than either calculated PDF due to the presence of a small amount of hydrogen from the incomplete deuteration of the sample that is not accounted for in either calculated PDF. The presence of hydrogen distorts the background most notably in the low r region and precludes meaningful fitting of the PDF that would normally allow extraction of information regarding short-range structure and domain size. Nonetheless, the PDF generated by simulation and extracted from the experimental data is in excellent agreement and suggests that future studies involving combined fitting of the experimental data and comparison with simulation will be fruitful.

The PDFs presented in Figure 8 bracket the structural phase transition at 225 K and span the radial distance corresponding to approximately six unit cells. Aside from slight differences in amplitude, the 220 and 230 K PDFs appear virtually identical and very similar to the 330 K PDF. Significant differences are seen in the PDFs between 100 and 220 K. In this temperature regime, the intermolecular bond distances are changing rapidly in the orthorhombic phase due to the changing lattice parameters and the progressive rotation of the B−N bond parallel to the c-axis. The PDF calculated from molecular simulation using a BLYP functional were compared (not shown) to that generated using a PBE functional at 220 K. Minor differences in PDF amplitudes were observed comparable to those generated by increasing the temperature by 10 K. Furthermore, the resulting PDF from larger 3 × 3 × 3 and 4 × 4 × 4 simulation cells were compared to the smaller 2 × 2 × 2 cell results, and no significant changes were observed.

Discussion

Rietveld Analysis and Molecular Simulation. Both intra- and intermolecular bond lengths and angles determined from Rietveld refinement compare well to those from molecular simulation in numerical value and temperature-dependent trends. In general, closer agreement was found between the mean field average and the uncorrected bond lengths from Rietveld refinement. This suggests that the mean field average provides a long-length scale representation similar to diffraction studies. In contrast, the metrics from ensemble averages display little temperature dependence and are in good agreement with the Rietveld values corrected for thermal motion, or riding motion, and precession. These results suggest that ensemble average provides a molecular length scale view. Both the correct Rietveld bond lengths and the ensemble average indicate that the ammonia borane molecule is insensitive to temperature across the temperature range investigated.

Nature of Orthorhombic to Tetragonal Phase Transition. Rietveld refinements of NPD data clearly indicate that the orthorhombic to tetragonal phase transition is preceded by progressive displacement of the borane group along the b-axis leading to the rotation of the B−N bond parallel to the c-axis, and the change in a and b lattice parameters occurs progressively in the orthorhombic phase. At the phase transition, rotational disorder of the hydrogen atoms in the borane and amine groups results in the tetragonal structure. Molecular dynamics simulation augments the visualization of this phase transition mechanism, with the precessional motion of the ammonia borane molecule leading to an apparent shortening of the B−N bond. Some features of the two-step transition mechanism observed in NH_3BH_3 are similar to the orthorhombic to cubic phase transition observed in C_2Cl_6 and C_2Br_6. In these compounds, Woost and Bougeard[40] proposed a two-step transition mechanism by which the C_2Cl_6 molecular three-fold axis becomes parallel to the cubic body diagonals. The first step involves high amplitude displacements about the a-axis normal to the three-fold axis, resulting in disorder in the $b-c$ plane commensurate with breaking the 90° angular relationship between the a- and c-axes, resulting in the creation of a monoclinic intermediate phase. The second step marks the onset of rotational disorder about the molecular three-fold axis leading to the development of the cubic phase. Potential evidence for an intermediate phase in ammonia borane was also found in Raman studies of the phase transition from the delayed appearance of vibrational modes predicted by group theory to 10 K below the phase transition temperature.[10] On the basis of the analysis of the NPD data, we find no evidence of an intermediate phase and a much simpler mechanism than that proposed for C_2Cl_6 and C_2Br_6.[40] The importance of a displacive component to the orthorhombic to tetragonal phase transition in ammonia borane was also recently recognized in a ^{15}N NMR study, although it was concluded that the librational motion of the amine group triggered the phase transition.[41]

Disorder of Amine and Borane Groups. Previous NMR and quasielastic neutron spectroscopic studies have determined one of the most distinguishing features of the orthorhombic to tetragonal phase transition is the dramatic change in the rotational dynamics of the amine and borane groups. The rotational energy barrier decreases by factors of 2 and 4 for the amine and borane groups, respectively.[42−44]

Quantitative measures of the magnitude of the order−disorder across the phase transition are difficult to obtain directly from the results of Rietveld refinement. In the orthorhombic phase, one can easily track the temperature-dependent increase in

atomic displacement parameters for the deuterium atoms in Table 2. However, in the tetragonal phase the magnitude of the deuterium atomic displacement parameters is influenced by the model chosen to represent the disorder, and as a result, direct comparison to orthorhombic parameters is not meaningful.

A visual representation of the impact of hydrogen dynamics contained in the diffraction data that is independent of the mathematical model chosen is possible from examination of the Fourier transform of the observed neutron scattering intensity from deuterium atoms, or DELF maps, as a function of temperature from refinements where only the nitrogen and boron atoms have nonzero occupancy. Typically, DELF maps are used to locate the positions of atoms that are missing from the refinement model; however, they can also be used to visualize the hydrogen disorder without bias from the mathematical representation of the number of sites and symmetry constrained shape of the ADP ellipsoids. Three-dimensional representations of the DELF maps at several temperatures are available in the Supporting Information.

At low temperature, the scattering intensity from the deuterium atoms forms well-isolated, ellipsoid-shaped volumes about the nitrogen and boron atoms and the three-fold molecular symmetry is readily apparent. At 120 K, the volumes about the nitrogen atom are distended. At the same temperature, the three volumes about the boron atom remain ellipsoid shaped. At 220 K, the volumes form discontinuous annular rings albeit with increased density at the orthorhombic atomic positions for the deuterium atoms. These observations correlate well with quasielastic neutron studies which indicate that the dynamics of the amine and borane hydrogen atoms increases markedly at ca. 110 and 220 K, respectively.[42,44] At temperatures above 230 K, in the tetragonal phase, both the borane and amine groups are represented by continuous annular rings.

Temperature-dependent changes in the atomic displacement parameters can also be extracted from the molecular dynamics simulations. The anisotropic atomic displacement parameters are derived from the statistical fluctuations observed in the atomic positions of the canonical ensembles at a given temperature. This approach has the obvious benefit of not being a symmetrically constrained representation and as a result provides insight into increased dynamics across the phase transition. The atomic displacement parameters are listed in Table 2, and visual representations are provided at several temperatures in the Supporting Information. These images are quite similar to the temperature-dependent trends observed for the DELF surfaces discussed above.

Dihydrogen Bonding Network. Of particular interest to the utilization of ammonia borane as a hydrogen storage material is the rapid, controlled release of H_2 at moderate temperatures. This requires understanding of the nature and the evolution of the dihydrogen bond network as a function of temperature and changes in lattice parameters and intramolecular geometry in the tetragonal phase. Using a 12-site model of the hydrogen disorder in the tetragonal phase, we have determined that the structural changes in the dihydrogen bonding network occurring at the phase transition temperature are modest, involving the breaking of D2···D4, a weak dihydrogen bond. This is also reflected in the relatively small transition enthalpy of 1.48 kJ mol^{-1} based on heat capacity measurements.[45]

Further evidence for weakening of remaining D2···D3 dihydrogen in the tetragonal phase comes from examination of the θ angle $\angle$BD3···D2. In a review of 26 compounds with N−H···H−B intermolecular dihydrogen bonds, the majority of θ angles $\angle$BH···H fell within the range of 95−115°.[2] This range differs only slightly from that observed in a recent gas phase study of dihydrogen bonds.[46] At 230 K, the θ angle $\angle$BD3···D2 becomes 119°, more obtuse than the majority of compounds with N−H···H−B dihydrogen bonds. If the intramolecular ammonia borane geometry stays constant with increasing temperature, then corresponding unit cell volume expansion will result in the lengthening of the D3···D2 bond. Additionally, since the unit cell expansion is dominated by the increase in *a* lattice parameters and not *c*, it will also result in further increases of θ angle $\angle$BD3···D2. In fact, extrapolation of the *a* and *c* lattice parameters to 380 K, the temperature at which H_2 is rapidly released, leads to D3···D2 bond length of 2.22 Å and θ angle $\angle$BD3···D2 of 120°, suggesting a significant weakening of the only remaining dihydrogen bond.

Conclusions

This study has revealed three interesting aspects of the temperature-dependent changes in the intra- and intermolecular structure of ammonia borane that could impact the dihydrogen bonding network. First, the intramolecular geometry changes little as a function of temperature and across the phase transition boundary even though the *a* and *b* lattice parameters are changing significantly and the unit cell volume increases over this temperature range, resulting in the creation of additional intermolecular space as the phase transition is approached. Second, the rotation of the B−N bond parallel to *c*-axis with increasing temperature is accomplished by the translation of borane group along the *b*-axis. Third, from molecular geometry arguments, it is apparent that the dihydrogen bonding network is significantly weaker in the tetragonal phase than in the orthorhombic phase and further weakening could precede the release of H_2.

These progressive displacive structural changes culminate in a dramatic change in the dynamics of the amine and borane groups at the phase transition defining the order−disorder transition to the tetragonal phase. Our ability to understand the nature of the disorder in the tetragonal phase from the viewpoint of Rietveld refinement of the NPD data was limited by symmetry constraints and the nature of long-length scale averages. Major insights were gained from the molecular dynamics simulation. These include the close correlation between results from mean field averages and those from Rietveld analysis, whereas ensemble averages appear to reflect the local molecular structural changes. Other significant insights from molecular dynamic simulations include the precession of the ammonia borane molecules about the *c*-axis and extraction of a set of anisotropic atomic displacement parameters across the temperature range investigated.

Acknowledgment. N.J.H. has greatly benefited from discussions with Drs. M.E. Bowden and W.I.F. David. This work was supported by the Office of Basic Energy Sciences Hydrogen Fuel Initiative, Chemical Sciences Division, of the U.S. Department of Energy. Pacific Northwest is operated for the Department of Energy by Battelle. A portion of the research described in this paper was performed in the Environmental Molecular Sciences Laboratory, a national scientific user facility sponsored by the Department of Energy's Office of Biological and Environmental Research and located at Pacific Northwest National Laboratory. The Lujan Center at Los Alamos Neutron Science Center is funded by Department of Energy, Office of Basic Energy Sciences. The upgrade of NPDF at Los Alamos has been funded by the National Science Foundation through Grant DMR 0076488.

Supporting Information Available: Diffractograms at 15, 220, 230, and 340 K, anisotropic displacement parameters

determined from Rietveld analysis of the NPD data, anistropic displacement parameters determined molecular simulation, three-dimensional isosurfaces constructed from DELF maps at multiple temperatures, and graphical representation of thermal ellipsoids based on molecular simulation at multiple temperatures. This material is available free of charge via the Internet at http://pubs.acs.org.

References and Notes

(1) Shore, S. G.; Böddeker, K. W. Large scale synthesis of $H_2B(NH_3)_2^+BH_4^-$ and H_3NBH_3. *Inorg. Chem.* **1964**, *3*, 914–915.

(2) Klooster, W. T.; Koetzle, T. F.; Siegbahn, P. E. M.; Richardson, T. B.; Crabtree, R. H. Study of the N−H···B−H dihydrogen bond including the crystal structure of BH_3NH_3 by neutron diffraction. *J. Am. Chem. Soc.* **1999**, *121*, 6337–6343.

(3) Hoon, C. F.; Reynhardt, E. C. Molecular dynamics and structures of amine borane of the type $R_3N{\cdot}BH_3$: I. X-ray investigation of the $H_3N{\cdot}BH_3$ at 295 K and 110 K. *J. Phys. C: Solid State Phys.* **1983**, *16*, 6129–6136.

(4) Wolf, G.; Baumann, J.; Baitalow, F.; Hoffmann, F. P. Calorimetric process monitoring of thermal decomposition of B−N−H compounds. *Thermochim. Acta* **2000**, *343*, 19–25.

(5) Stowe, A. C.; Shaw, W. J.; Linehan, J. C.; Schmid, B.; Autrey, T. In situ solid state ^{11}B MAS-NMR studies of the thermal decomposition of ammonia borane: mechanistic studies of the hydrogen release pathways from a solid state hydrogen storage material. *Phys. Chem. Chem. Phys.* **2007**, *9*, 1831–1836.

(6) Heldebrant, D. J.; Karkamkar, A.; Hess, N. J.; Bowden, M.; Rassat, S.; Zheng, F.; Rappe, K.; Autrey, T. The effects of chemical additives on the induction phase in solid-state thermal decomposition of ammonia borane. *Chem. Mater.* **2008**, *20*, 5332–5336.

(7) Mauder, T. B. Will we soon be fueling our automobiles with ammonia-borane. *Angew. Chem., Int. Ed.* **2007**, *46*, 8116–8118.

(8) Yang, J. B.; Lamsal, J.; Cal, Q.; James, W. J.; Yelon, W. B. Structural evolution of ammonia borane for hydrogen storage. *Appl. Phys. Lett.* **2008**, *92*, 091916.

(9) Bowden, M. E.; Gainsford, G. J.; Robinson, W. T. Room temperature structure of ammonia borane. *Aust. J. Chem.* **2007**, *60*, 149–153.

(10) Hess, N. J.; Parvanov, V. M.; Mundy, C.; Kathmann, S. M.; Schenter, G. K.; Autrey, T. Spectroscopic studies of the phase transition in ammonia borane: Raman spectroscopy of single crystal NH_3BH_3 as a function of temperature from 88 to 330 K. *J. Chem. Phys.* **2008**, *128*, 034508.

(11) Brown, C. M.; Jacques, T. L.; Hess, N. J.; Daemen, L. L.; Mamontov, E.; Stowe, A. C.; Autrey, T. Dynamics of ammonia borane using neutron scattering. *Physica B* **2006**, *385*, 266–268.

(12) The 8-site model does not preserve the C_{3v} symmetry because the hydrogen positions are spaced 45° apart, whereas C_{3v} requires 120° separation, which is not a multiple of 45°. In the 12-site model, the hydrogen positions are spaced 30° apart thus consistent with C_{3v} symmetry.

(13) van Nes, G. J. H.; Vos, A. Single-crystal structures and electron density distributions of ethane, ethylene, and acetylene: I. Single crystal X-ray structure determinations of two modifications of ethane. *Acta Crystallogr., Sect. B* **1978**, *34*, 1947–1956.

(14) Hohlwein, D.; Nägele, W.; Prandl, W. Neutron structure refinement of orthorhombic hexachloroethane. *Acta Crystallogr., Sect. B* **1979**, *35*, 2975–2978.

(15) Mandel, G.; Donohue, J. The refinement of the structure of hexabromoethane. *Acta Crystallogr., Sect. B* **1972**, *28*, 1313–1316.

(16) Gerlach, P.; Hohlwein, D.; Prandl, W.; Schulz, F. W. The plastic phase of hexachloroethane, C_2Cl_6: a neutron powder and single-crystal investigation. *Acta Crystallogr., Sect. A* **1981**, *37*, 904–908.

(17) Koide, T.; Tsujino, M.; Sawada, K.; Oda, T. Phase transition of solid hexabromoethane. *Bull. Chem. Soc. Jpn.* **1974**, *47*, 2998–3000.

(18) Parvanov, V. M.; Schenter, G. K.; Hess, N. J.; Daemen, L. L.; Hartl, M.; Stowe, A. C.; Camaioni, D. M.; Autrey, T. Materials for hydrogen storage: structure and dynamics of borane ammonia complex. *Dalton Trans.* **2008**, *33*, 4514–4522.

(19) Subsequent NMR and Raman analysis indicated that borane group was incompletely deuterated and contained 15% hydrogen. To account for the partial deuteration of the borane group in the Rietveld refinement, the scattering length for these atoms was set at 0.5109 fm.

(20) Proffen, Th.; Egami, T.; Billinge, S. J. L.; Cheetham, A. K.; Louca, D.; Parise, J. B. *Appl. Phys. A: Mater. Sci. Process.* **2002**, *74*, S163.

(21) Rietveld, H. M. Line profiles of neutron powder-diffraction peaks for structure refinement. *Acta Crystallogr.* **1967**, *22*, 151–152.

(22) Larson, A. C.; Von Dreele, R. B. General structure analysis systems (GSAS). Los Alamos National Laboratory Report LAUR 86-7498, **1974**.

(23) Toby, B. H. EXPGUI, a graphical user interface for GSAS. *J. Appl. Crystallogr.* **2001**, *34*, 210–213.

(24) Schomaker, V.; Trueblood, K. N. On the rigid-body motion of molecules in crystals. *Acta Crystallogr., Sect. B* **1968**, *24*, 63–76.

(25) Peterson, P. F.; Gutmann, M.; Proffen, Th.; Billinge, S. J. L. PDFgetN: A user-friendly program to extract the total scattering structure function and the pair distribution function from neutron powder diffraction data. *J. Appl. Crystallogr.* **2000**, *33*, 1192.

(26) Proffen, Th.; Billinge, S. J. L. PDFFIT, a program for full profile structural refinement of the atonic pair distribution function. *J. Appl. Crystallogr.* **1999**, *32*, 572.

(27) Perdew, J. P.; Burke, K.; Ernzerhof, M. *Phys. Rev. Lett.* **1996**, *77*, 3865.

(28) Hartwigsen, C.; Goedecker, S.; Hutter, J. Relativistic separable dual-space Gaussian pseudopotentials from H to Rn. *Phys. Rev. B* **1998**, *58*, 3641.

(29) Goedecker, S.; Teter, M.; Hutter, J. Separable dual-space Gaussian pseudopotentials. *Phys. Rev. B* **1996**, *54*, 1703.

(30) Miranda, C. R.; Ceder, G. Ab initio investigation of ammonia-borane complexes for hydrogen storage. *J. Chem. Phys.* **2007**, *126*, 184703.

(31) Hutter, J.; Curioni, A. Car−Parrinello molecular dynamics on massively parallel computers. *Chemphyschem* **2005**, *6*, 1788–1793.

(32) VandeVondele, J.; Hutter, J. An efficient orbital transformation method for electronic structure calculations. *J. Chem. Phys.* **2003**, *118*, 4365.

(33) VandeVondele, J.; Krack, M.; Mohamed, F.; Parrinello, M.; Chassaing, T.; Hutter, J. QUICKSTEP: Fast and accurate density functional calculations using a mixed Gaussian and plane waves approach. *Comput. Phys. Commun.* **2005**, *67*, 103–128.

(34) Lippert, G.; Hutter, J.; Parrinello, M. A hybrid Gaussian and plane wave density functional scheme. *Mol. Phys.* **1997**, *92*, 477.

(35) The average B−D bond length is calculated as [(B−D3) + 2*(B−D4)]/3, and the associated uncertainty plotted is the uncertainty calculated for the B−D3 bond length, which in all cases is the larger than that of the B−D4 bond length, similarly for the average N−D bond length. The choice of the more conservative uncertainty results in error bars that are comparable to the size of the plotted data point.

(36) Busing, W. R.; Levy, H. A. The effect of thermal motion on the estimation of bond lengths from diffraction measurements. *Acta Crystallogr.* **1964**, *17*, 142–146.

(37) Rousseau, R.; Boero, M.; Bernasconi, M.; Parrinello, M.; Terakura, K. Static structure and dynamic corrections in high pressure H_2S. *Phys. Rev. Lett.* **1999**, *83*, 2218–2221.

(38) The following analysis is based on uncorrected N−D and B−D bond lengths from Rietveld analysis. Corrections for thermal motions would result in slightly shorter dihydrogen bonds.

(39) Kar, T.; Scheiner, S. Comparison between hydrogen and dihydrogen bonds among H_3BNH_3, H_2BNH_2, and NH_3. *J. Chem. Phys.* **2003**, *119*, 1473–1482.

(40) Woost, B.; Bougeard, D. *J. Chem. Phys.* **1986**, *84*, 4810.

(41) Gunayden-Sen, O.; Achey, R.; Dalal, N. S.; Stowe, A.; Autrey, T. High resolution ^{15}N NMR of the 225 K phase transition in ammonia borane (NH_3BH_3): mixed order-disorder and displacive behavior. *J. Phys. Chem. B* **2007**, *111*, 677–681.

(42) Brown, C. M.; Jacques, T. L.; Hess, N. J.; Daemen, L. L.; Mamontov, E.; Stowe, A. C.; Autrey, T. Dynamics of ammonia borane using neutron scattering. *Physica B* **2006**, *385*, 266–268.

(43) Penner, G. H.; Chang, Y. C. P.; Hutzal, J. A deuterium NMR spectroscopic study of solid BH_3NH_3. *Inorg. Chem.* **1999**, *38*, 2868–2873.

(44) Hess, N. J.; Hartman, M. R.; Brown, C. M.; Mamontov, E.; Karkamkar, A.; Heldebrant, D. J.; Daemen, L. L.; Autrey, T. Quasielastic neutron scattering of $-NH_3$ and $-BH_3$ rotational dynamics in orthorhombic ammonia borane. *Chem. Phys. Lett.* **2008**, *458*, 85–88.

(45) Wolf, G.; van Miltenburg, J. C.; Wolf, U. Thermochemical investigations on borazane (BH_3-NH_3) in the temperature range from 10 to 289 K. *Thermochim. Acta* **1998**, *317*, 111–116.

(46) Kar, T.; Scheiner, S. Comparison between hydrogen and dihydrogen bonds among H_3BNH_3, H_2BNH_2, and NH_3. *J. Chem. Phys.* **2003**, *119*, 1473–1482.

JP900839C